Hindawi
Journal of Nanomaterials
Volume 2019, Article ID 8928917, 13 pages
https://doi.org/10.1155/2019/8928917

Research Article

Enhancement of Through-Thickness Thermal Transport in Unidirectional Carbon Fiber Reinforced Plastic Laminates due to the Synergetic Role of Carbon Nanofiber Z-Threads

Alexander M. Scruggs, Sebastian Kirmse, and Kuang-Ting Hsiao

Department of Mechanical Engineering, University of South Alabama, Mobile, AL 36688, USA

Correspondence should be addressed to Kuang-Ting Hsiao; kthsiao@southalabama.edu

Received 30 July 2018; Accepted 21 October 2018; Published 3 January 2019

Academic Editor: Victor M. Castaño

This study experimentally and analytically examined the influence of carbon nanofiber (CNF) z-threads on the through-thickness (i.e., z-direction) thermal conductivity of unidirectional carbon fiber reinforced plastics (CFRPs). It was hypothesized that a network of CNF z-threads within CFRPs would provide a thermally conductive microstructure throughout the sample thickness that would increase the through-thickness thermal conductivity. The experiments showed that the through-thickness thermal conductivity of the CNF z-threaded CFRPs (9.85 W/m-K) was approximately 7.53 times greater than that of the control CFRPs (1.31 W/m-K) and 2.73 times greater than that of the unaligned CNF-modified CFRPs (3.61 W/m-K). Accordingly, the CNF z-threads were found to play a substantial role in increasing the through-thickness thermal conductivity of CFRPs. To better understand the role of the CNF z-threads in through-thickness thermal transport, simple logical models of the CFRPs were constructed and then compared with the experimental results. Through these analyses, it was determined that CNF z-threads substantially enhance the through-thickness thermal conductivity by creating carbon fiber-CNF linkages throughout the CFRP laminate; these linkages allow the heat flow to largely bypass the resistive resin that envelops the carbon fibers. In addition, thermal infrared tests illustrated that the increased through-thickness thermal conductivity of the CNF z-threaded CFRP enabled the location and visualization of defects within the laminate, which was not possible with the control CFRP.

1. Introduction

Carbon fiber reinforced plastics (CFRPs) exhibit high modulus-to-weight and strength-to-weight ratios, which makes them particularly desirable for use in industries where weight-savings is critical, such as the aerospace and automotive industries. However, the absence of z-direction fiber reinforcement in CFRPs results in the polymer matrix material dominating the z-direction performance of the laminate. Moreover, polymer matrices typically have very low thermal conductivity. Therefore, under good fiber-wetting conditions, the polymer matrix acts as an insulating barrier that surrounds individual carbon fibers. Accordingly, CFRPs tend to have relatively poor z-direction thermal conductivity (approximately 1 W/m-K) in comparison to their in-plane thermal conductivity (approximately 10 W/m-K) [1–4].

If utilized effectively, the high aspect ratio of carbon nanofibers (CNFs) enables the potential formation of a multiscale network throughout the composite structure. Furthermore, as high heat-treated (HHT) carbon nanofibers possess a thermal conductivity value of approximately 1950 W/m-K [5], CNFs have the potential to substantially enhance the through-thickness thermal conductivity of CFRPs. For comparison, the thermal conductivity of an AS4 carbon fiber tow is approximately 6.83 W/m-K [6], and the thermal conductivity of stainless steel is approximately 15.26 W/m-K [7]. However, the ideal thermal properties of CNFs have not been effectively translated into increases in the macroscale properties of CFRPs due to technical barriers regarding the processing and positioning of CNFs. Most studies that involve the creation of multiscale reinforcements within FRPs by using high aspect ratio carbon-based

nanoparticles (e.g., carbon nanofibers, carbon nanotubes) have dispersed the nanoparticles in a matrix material and then impregnating a fiber system with the nanoparticle-enhanced matrix material [8–11]. Despite the commonality of the dispersion-impregnation process, it is inundated with issues in both nanoparticle dispersion and orientation.

To circumvent the challenges associated with the dispersion-impregnation approach, chemical vapor deposition (CVD) has been utilized in other studies to grow carbon nanotubes (CNTs) directly on the surface of a fiber system, thereby creating a radially aligned CNT nanostructure. While this method has produced substantial enhancements in electrical, mechanical, and thermal properties of ceramic (e.g., alumina) fiber-reinforced plastics [4, 12–14], it is not traditionally compatible with carbon fabrics due to exposure to high temperatures and metal catalysts. Recently, a preliminary study [15] has shown that a radially aligned CNT nanostructure can be grown on the surface of carbon fibers; however, this study does not include any laminate level testing, so comparisons to CFRPs constructed with other methods are not yet possible. In addition, CNTs deposited on dry fibers can be cumbersome to handle. As such, an alternative to the dispersion-impregnation approach is still required to create multiscale reinforcements in CFRPs with controlled nanoparticle dispersion and orientation.

The necessity for multiscale reinforcements in CFRPs that utilize high aspect ratio nanoparticles led to the recent development of CNF z-threaded CFRPs (ZT-CFRPs) [16], which utilize the desirable length of CNFs (approximately 10-100 times longer than the carbon fiber diameter) to achieve a long-range threading effect in the carbon fiber array. The z-threaded CNF network within ZT-CFRPs has been shown to increase both interlaminar fracture toughness [16] and through-thickness electrical conductivity [17, 18]; however, no previous studies have characterized the contribution of these CNF z-threads on thermal transport in the z-direction. This paper experimentally and analytically investigates the effect and role of CNF z-threads regarding through-thickness thermal conductivity enhancement of unidirectional CFRPs.

2. Materials and Methods

2.1. Materials. In this study, 18-ply and 27-ply CFRP laminates of the following three sample types were constructed: unmodified CFRPs (control CFRPs), CFRPs with 1 wt% unaligned CNFs (UA-CFRPs), and CFRPs with 1 wt% CNF z-threads (ZT-CFRPs); CNF concentration was measured as a percentage of matrix weight. Note that the 1 wt% CNF concentration was selected by a trial-and-error process as the highest concentration for consistent alignment quality. The CFRPs were constructed from a Hexcel AS4 unidirectional fabric (190 g/m^2 areal weight, 3 K tow) and a two-part epoxy from Momentive that consists of Epon 862 resin (a diglycidyl ether of bisphenol F) and Epikure W catalyst (a non-MDA aromatic amine curing agent that contains diethylmethylbenzenediamine). The CNFs used in this study were PR-24-XT-HHT carbon nanofibers (Pyrograf Products, Inc.), which possess an average diameter of 100 nm and lengths ranging from 50 μm to 200 μm [19]. Approximately 1 wt% of both Disperbyk-191 and Disperbyk-192 surfactants (BYK) was added to the resin to assist CNF dispersion [20].

2.2. CFRP Laminate Preparation. The CFRP prepregs used in this study were fabricated using the methods described in Figure 1; note that these steps are described in further detail by the authors in a previous study [16]. The prepreg manufacturing processes used in this study, including both the hand wet lay-up process (used for the control CFRPs and the UA-CFRPs) and the sponge transfer process (used for the ZT-CFRPs), were performed on single plies of carbon fabric to minimize any potential particle filtering effect. The single-ply prepregs can then be cut into several pieces, which can be stacked and then cured into laminates of various thicknesses.

The individual single-ply prepregs were cut into 50 mm × 50 mm squares and stacked on a release agent-coated aluminum plate to create 18-ply and 27-ply samples of each sample type. After stacking, the prepregs were covered by a layer of peel ply and two layers of distribution media. Two vacuum channels equipped with high-temperature vacuum lines were then placed on top of the distribution media, and then, sealant tape was placed on the edges of the aluminum mold to anchor a layer of vacuum bagging. After vacuum was drawn on the samples, the mold was placed in a hot press, and the heated plates were closed until only a small gap remained between the top heating plate and the aluminum mold; this emulated an even-heating oven environment, which is typical of an out of autoclave-vacuum bag only (OOA-VBO) curing process.

The following steps outline the OOA-VBO cure cycle used to create the samples in this study: (1) the samples were placed under vacuum (approximately 1 bar) and then kept at 23°C (i.e., room temperature) for 60 minutes; (2) the mold temperature was increased to 45°C, and then the mold was subjected to a 30-minute isothermal dwell; (3) the mold temperature was then increased to 120°C, and then, mold was subjected to a 120-minute isothermal dwell; and (4) vacuum was released on the mold, the mold temperature was increased to 180°C, and then the mold was subjected to a final 240-minute isothermal dwell.

After demolding, the CFRP samples were trimmed using a table saw that was equipped with a diamond blade. Before testing, the surfaces of the CFRP were lightly polished and then subsequently cleaned with acetone to remove any particles that accumulated on the sample during cutting and surface preparation.

2.3. Thermal Conductivity Testing. Figure 2 presents a schematic of the steady-state measurement device used to determine the thermal conductivity of each sample. Note that the measurement device used in this study was adapted from a previous system that was designed to test the thermal conductivity of solid-phase paraffin wax [21]. A heat source, two thermoelectric coolers, and two fans were regulated using LabVIEW in order to maintain two aluminum heat sinks at constant temperature; the bottom aluminum plate was maintained at 50°C, whereas the top aluminum plate

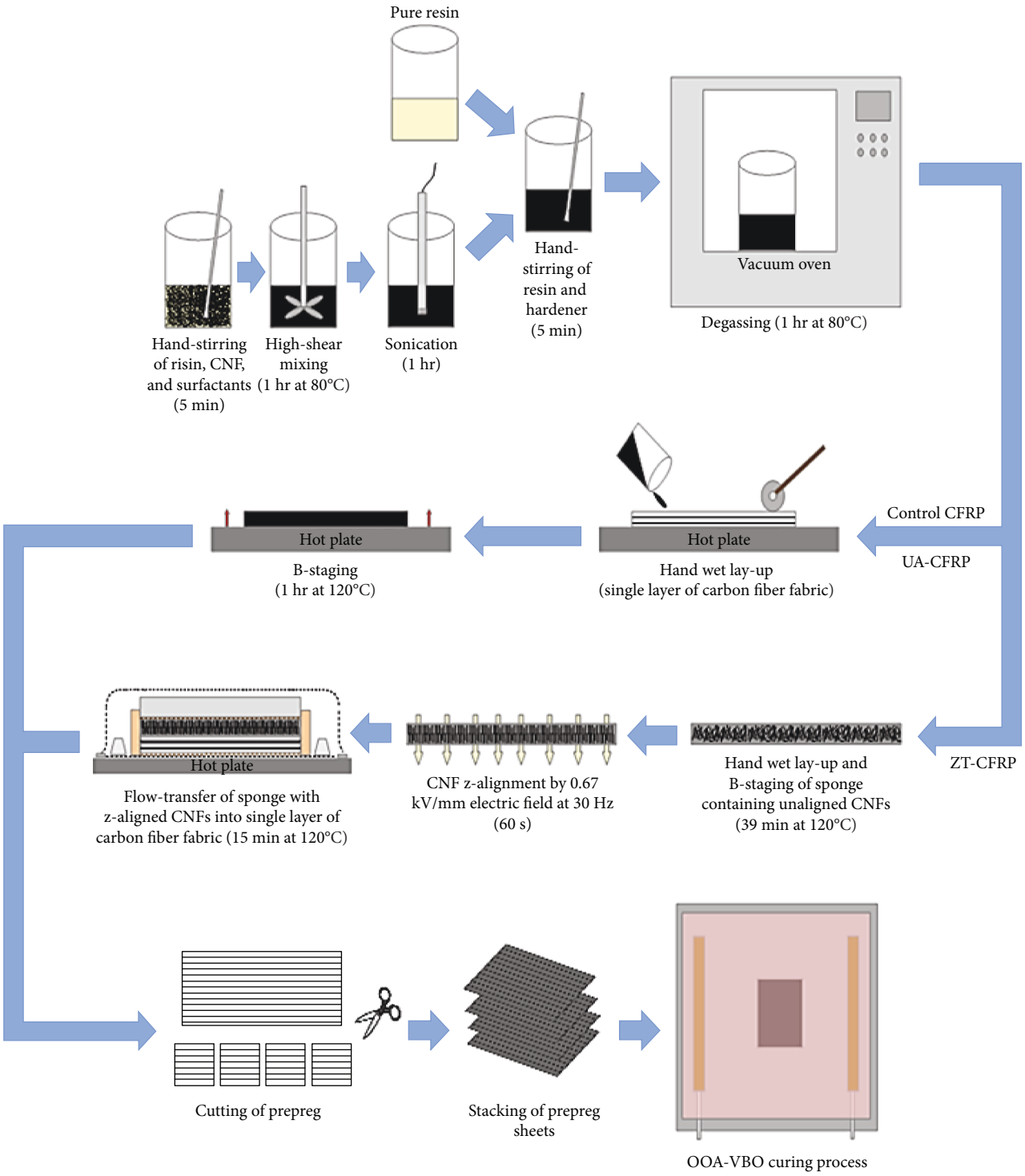

Figure 1: CFRP prepreg manufacturing process.

was maintained at 20°C. The heat flux on either side of the sample was measured by two heat flux sensors with embedded T-type thermocouples, which were positioned on either side of the sample. Four additional T-type thermocouples—two thermocouples on the top surface of the tested sample and two thermocouples on the bottom surface—provided a more accurate measure of the temperature drop through the sample thickness. To ensure the measured values were as consistent as possible, three independent measurements were taken for each sample.

Equation (1) illustrates the heat flux conducted through a flat plate with no heat generation, which was used together with Fourier's Law to solve for the thermal conductivity of the sample, as shown in Eq. (2). Accordingly,

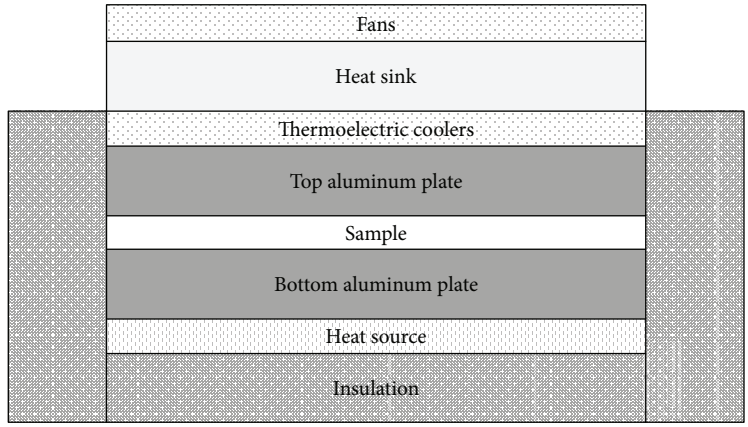

Figure 2: Schematic of steady-state thermal conductivity testing device.

Table 1: Through-thickness thermal conductivity sample statistics. Note that $\bar{x}$ is the sample mean, s is the sample standard deviation, C.V. is the coefficient of variation ($s/\bar{x}$), and μ is the population mean.

Sample type	$\bar{x}$ (W/mK)	s (W/mK)	*C.V.* (%)	Carbon fiber volume fraction (%)
Paraffin wax	2.73E-01	1.53E-03	0.56	N/A
Control CFRPs	1.31	2.63E-02	2.01	76.73 (18-ply) 75.37 (27-ply)
1 wt% UA-CFRPs	3.61	9.38E-02	2.60	68.24 (18-ply) 68.22 (27-ply)
1 wt% ZT-CFRPs	9.85	2.37E-01	2.40	71.83 (18-ply) 71.78 (27-ply)
304 stainless steel	15.22	2.21E-01	1.45	N/A

the data collected from the thermal conductivity measurement device were inserted into Eq. (2) to solve for the thermal conductivity of each sample.

$$q = \frac{\Delta T}{\sum AR} = \frac{\Delta T}{AR_{\text{sample}} + AR_{\text{contact}}}, \quad (1)$$

$$k_{\text{sample}} = \frac{L_{\text{sample}}}{(\Delta T/q) - AR_{\text{contact}}}. \quad (2)$$

In the equations above, q is the heat flux through the sample thickness (W/m^2), ΔT is the temperature drop across the sample, L_{sample} is the sample thickness (m), A is the sample area (m^2), and R_{sample} is the through-thickness thermal resistance (K/W) for the sample; AR_{sample} is the thermal insulance (m^2 K/W), which is defined as the thermal resistance of a unit area of sample, and therefore, it is independent from the actual area of each sample being tested. Additionally, note that the effect of thermal contact insulance between the sample and the aluminum plates (top plate and bottom plate) was lumped into AR_{contact}.

For each sample type, two laminates of different thicknesses (i.e., 18-ply sample and 27-ply sample) were tested three times to obtain independent steady-state temperature drop (ΔT) and heat flux (q) values. Since both samples were created from the same material system and the carbon fiber volume fractions were approximately equal (as shown in Table 1), it was assumed that both samples had identical thermal conductivity (k_{sample}) and thermal contact insulance (AR_{contact}). If the thermal conductivities of both samples are identical, the thermal insulance for each sample (AR_{sample}) differs solely by a factor of the respective sample thicknesses ($R_1/R_2 = L_1/L_2$). Hence, one can solve for the k_{sample} and AR_{contact} terms found in Eq. (2) by using the three sets of data measured from each of the two samples.

2.4. CNF Microstructure Characterization. The respective microstructures of the CNF networks contained within the UA-CFRPs and ZT-CFRPs were characterized and compared using an FEI Quanta 250 environmental scanning electron microscope (ESEM).

3. Results and Discussion

3.1. Through-Thickness Thermal Conductivity. Once the CFRP laminates had been tested, the through-thickness thermal conductivity k_{sample} of each was determined using Eq. (2), and then the results were statistically analyzed. Table 1 presents the summary comparing the through-thickness thermal conductivity of each respective sample type (i.e., control CFRPs, 1 wt% UA-CFRPs, and 1 wt% ZT-CFRPs). In addition, to ensure the measurement setup was

accurate within the testing range, samples of two different materials (i.e., paraffin wax and 304 stainless steel) with known thermal conductivity values that cover the range of interest were also tested. According to literature, the thermal conductivities of paraffin wax and 304 stainless steel (at 25°C) are approximately 2.70E-01 W/m-K [22] and 15.26 W/m-K [7], respectively. The measurements by the setup for paraffin wax (three sample thicknesses of 3.10 mm, 5.16 mm, and 5.88 mm) and 304 stainless steel (two sample thicknesses of 3.18 mm and 6.35 mm) were 0.273E-01 W/m-K and 15.22 W/m-K, respectively. The relative difference between the measurements and published data were +1.11% and −0.26% for paraffin wax and 304 stainless steel, respectively. Thus, the results acquired from the measurement system used in this study were reasonably accurate within the range of interest.

According to the roles of CNFs regarding thermal transport in CFRPs, it was hypothesized that (i) CNFs would increase CFRP through-thickness thermal conductivity and that (ii) CNF z-threads would yield a greater improvement in CFRP through-thickness thermal conductivity than that of the unaligned CNFs. Table 1 illustrates that both hypotheses were confirmed. The through-thickness thermal conductivity of the 1 wt% UA-CFRP was approximately 2.76 times greater than that of the control CFRP, which confirms the first hypothesis. In addition, the through-thickness thermal conductivity of the 1 wt% ZT-CFRP was approximately 7.53 times greater than that of the control CFRP and approximately 2.73 times greater than that of the 1 wt% UA-CFRP, which confirms the second hypothesis. By comparing the respective contributions of CNF addition and CNF orientation control, it was observed that CNF addition increased the thermal conductivity by 2.30 W/m-K, whereas the z-threading pattern contributed an additional 6.24 W/m-K.

At 9.85 W/m-K, the through-thickness thermal conductivity of the 1 wt% ZT-CFRP is notably greater than other unidirectional CFRPs reported in the literature, as illustrated in Table 2. Moreover, at 1 wt% CNF concentration, the thermal conductivity of the ZT-CFRP approaches the in-plane thermal conductivity of CFRP (~10 W/m-K) [4]. This finding indicates that the long-range CNF z-threads can effectively provide CFRP laminates with isotropic thermal conductivity, even though the continuous carbon fibers are exclusively oriented in the in-plane directions.

3.2. CNF Microstructure. Delamination surfaces from each sample type were prepared to observe and compare the CNF microstructures within the UA-CFRPs and ZT-CFRPs. As this analysis intended to highlight the difference between a typical unaligned CNF network and the CNF network created by CNF z-threads, it was imperative first to understand how to distinguish between the respective CNF networks when viewing the micrographs.

Figure 3 depicts the proposed CNF z-threading patterns within a CFRP, which helps illuminate the possible morphology of CNF z-threads in a delaminated CFRP laminate. The delamination surface is likely to occur at the necking gap between carbon fibers. Moreover, the matrix near the delamination surface is prone to shattering due to the interaction with the CNF z-threads under tension. Due to their orientation, broken CNF z-threads located at the delamination surface should only have one root in the matrix material and one broken tip. However, as a result of the zig-zag threading pattern, the local angle of a CNF z-thread may not be perfectly orthogonal to the delamination surface.

Upon examination of the UA-CFRP delamination surface shown in Figure 4, one can observe that the majority of the observed CNFs either have two roots in the matrix or they are oriented in the x-y plane, which indicates that they are not z-threads. On the other hand, the ZT-CFRP delamination surface shown in Figure 5 displays an organized CNF network z-threading through the thickness of the laminate.

Due to the strong mechanical interlocking associated with the zig-zag threading pattern illustrated in Figure 3, the CNF z-threads fracture very close to the matrix material; this phenomenon makes it difficult to see the CNF network from a top view of the delamination surface. As such, the SEM sample holding stage was rotated by 25 degrees to obtain an oblique view of a fiber tow that was partially split from the delamination surface, as shown in Figure 6. In this micrograph, one can observe a substantial number of CNF z-threads as well as their relationship with the carbon fibers.

As illustrated by the SEM micrographs, the majority of CNFs present within the UA-CFRPs were oriented in the x-y plane, whereas the network of CNF z-threads present in the ZT-CFRP extended throughout the CFRP laminate in the z-direction. With this observation, one can reasonably assume that CNF z-threads should have a greater impact on the thermal conductivity of CFRPs than that of unaligned CNFs since the incorporated CNFs are oriented in the z-axis. As such, the CNF z-threads are more capable of forming long-range conductive paths through the laminate than unaligned CNFs. Moreover, as the CNF z-threads zig-zag throughout the thickness of the CFRP, they link carbon fibers that would otherwise be separated by an epoxy barrier. This fiber-fiber linkage created by the CNF z-threads establishes a thermally conductive pathway throughout the thickness of the laminate. It is this synergy between the CNF z-orientation and the corresponding fiber-fiber linkage that produces the substantial increase in the through-thickness thermal conductivity, despite the low CNF concentration (1 wt% of the matrix translates to approximately 0.2 vol% of a CFRP with 70% carbon fiber volume fraction). Accordingly, the CNF z-threads are incredibly effective in enhancing z-directional heat conduction.

3.3. Model-Based Synergy Analysis of CNF Z-Threads. To build upon the knowledge regarding the contributions of the CNFs (either unaligned or z-threaded) to through-thickness thermal transport, simple logical models were used to help elaborate the roles of CNFs in the CFRPs. For these models, the CFRPs were represented by the following three components: carbon fiber, resin, and carbon nanofiber, which are denoted with the subscripts "CF," "R," and "CNF," respectively. The volume fractions of carbon fiber,

Table 2: Comparison of CFRP through-thickness thermal conductivity reported in the literature.

Data source	Unmodified CFRPs (control samples)				Nanoparticle-modified CFRPs		
	Fiber type	Layup	Fiber volume fraction	k (W/m-K)	Nanoparticle type	Nanoparticle concentration	k (W/m-K)
[11]	T300 UD	UD	58%	0.65	MWCNT	1 wt%	0.63
						3 wt%	0.62
					GNP	1 wt%	0.65
						3 wt%	0.68
						5 wt%	0.73
						10 wt%	0.86
						15 wt%	0.96
[23]	Sigmatex 2/2 TW	Plain weave	45%	0.39	GNP	1 vol%	0.42
					SNP	0.05 vol%	0.46
					SNW	0.05 vol%	0.42
					GNP/SNP	0.95 vol%/0.05 vol%	0.54
					GNP/SNW	0.95 vol%/0.05 vol%	0.54
[24]	SIGRAFIL® CE 1222-255-37 UD prepreg	UD	60%	1.07	Carbon black dispersed in ethylene glycol monomethyl ether	0.4 wt%	2.27
						0.6 wt%	2.40
						0.8 wt%	3.34
						1.0 wt%	2.15
						1.2 wt%	1.54
		Crossply	60%	1.04		0.4 wt%	1.76
						0.6 wt%	1.96
						0.8 wt%	2.23
						1.0 wt%	1.87
						1.2 wt%	1.60
[25]	Pyrofil TR50S UD	Crossply (0.1 MPa curing pressure)	58%	0.729	Carbon black	0.8 wt%	0.89
					SWCNT	0.4 wt%	0.91
					Chopped K-1100 carbon fiber	0.8 wt%	0.90
		Crossply (2.0 MPa curing pressure)	65%	1.091	Carbon black	0.8 wt%	1.21
					SWCNTs	0.4 wt%	1.45
					Chopped K-1100 carbon fiber	0.8 wt%	1.44
[26]	T300-40D PW	Plain weave	65%	0.77	Aligned MWCNT/epoxy interleaves	18-22 vol% (3 unmodified plies & 2 interleaves)	1.10
						18-22 vol% (7 unmodified plies & 6 interleaves)	1.18
This study	AS4 UD	UD	76%	1.308	HHT CNF (unaligned)	1 wt%	3.61
					HHT CNF z-threads	1 wt%	9.85

UD: unidirectional; GNP: graphite nanoplatelet; SNW: silver nanowire; SNP: silver nanoparticle; MWCNT: multiwalled carbon nanotube; SWCNT: single-walled carbon nanotube.

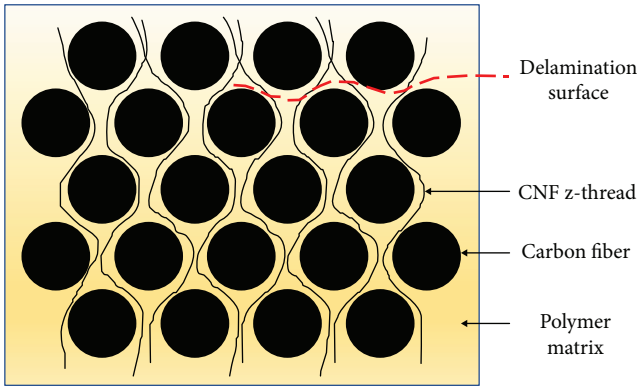

Figure 3: Proposed CNF z-threading patterns within a CFRP.

resin, and carbon nanofiber are denoted as V_{CF}, V_R, and V_{CNF}, respectively. During experimentation, the carbon fiber volume fraction was measured. Hence, the volume fractions of the carbon nanofiber (Eq. (3)) and the resin (Eq. (4)) can be calculated by using the CNF weight fraction in the resin ($w_{CNF} = 0.01$), the resin density ($\rho_R = 1.2003$ g/cm^3 [27]), and the CNF density ($\rho_{CNF} = 2.1$ g/cm^3 [5]), as shown hereafter.

$$V_{CNF} = (1 - V_{CF}) \frac{w_{CNF}/\rho_{CNF}}{w_{CNF}/\rho_{CNF} + w_R/\rho_R}, \quad (3)$$

$$V_R = 1 - V_{CF} - V_{CNF}. \quad (4)$$

All CFRP sample types (control CFRPs, UA-CFRPs, and ZT-CFRPs) were modeled with a carbon fiber volume fraction of 72.03%, which was the average carbon fiber volume fraction of all the samples. Accordingly, the volume fractions of the CNF and the resin are 0.16% and 27.81%, respectively.

The thermal conductivities of carbon fiber, resin, and carbon nanofiber are denoted as k_{CF}, k_R, and k_{CNF}, respectively. Although the thermal conductivity of a single carbon fiber is very difficult to measure, a rough estimate can still be made to assist in this analysis. According to the yarn/tow characteristics provided by Hexcel [6], the thermal conductivity of the AS4 HexTow is 6.83 W/m-K. Therefore, if a dry AS4 carbon fiber tow has a porosity of 40%, the thermal conductivity of a single carbon fiber is approximately 11.38 W/m-K. The thermal conductivities of the resin and CNF are 0.224 W/m-K [28] and 1950 W/m-K [5], respectively. Having estimated the necessary attributes of the CFRP components, one can attempt to model the thermal conductivities of the control CFRPs, UA-CFRPs, and ZT-CFRPs and hopefully discover the role of CNFs in the composites.

It is well known that the effective thermal conductivity of a mixture is constrained by the Wiener bounds. The Wiener lower bound of effective conductivity occurs when all three components are arranged in series (i.e., CF-R-CNF), as shown in

$$k_{e,[CF-R-CNF]} = \frac{1}{(V_{CF}/k_{CF}) + (V_R/k_R) + (V_{CNF}/k_{CNF})}. \quad (5)$$

The Wiener upper bound of the effective conductivity occurs when all three components are arranged in parallel (i.e., CF//R//CNF), as shown in

$$k_{e,[CF//R//CNF]} = V_{CF}k_{CF} + V_R k_R + V_{CNF}k_{CNF}. \quad (6)$$

Note that the parallel-model ($k_{e,[CF//R//CNF]}$) is not a realistic representation of the actual multiscale composite system since each carbon fiber is enveloped by the resin, which forms an insulating barrier; therefore, the carbon fibers cannot form a complete carbon conductive path in the through-thickness direction due to the presence of the insulating resin. Based on this shortfall, one might consider using CNFs, either unaligned or aligned, to improve the effective thermal conductivity of the control CFRPs ($k_{e,ControlCFRP}$), which was determined via experimentation to be 1.31 W/m-K. Moreover, one could consider the relationship between the control CFRP and CNFs as either a series or parallel arrangement, which form the two semiempirical models shown in

$$k_{e,[Control\,CFRP-CNF]} = \frac{1}{((V_{CF} + V_R)/k_{Control\,CFRP}) + (V_{CNF}/k_{CNF})}, \quad (7)$$

$$k_{e,[Control\,CFRP//CNF]} = (V_{CF} + V_R)k_{Control\,CFRP} + V_{CNF}k_{CNF}. \quad (8)$$

To further explore the interaction among the carbon nanofibers, resin, and carbon fibers, additional models were built with various series and parallel arrangement combinations among the three components. As the carbon fiber is always wrapped either by resin or by resin-CNF mixture, the models must allow the carbon fiber to form a series arrangement with the resin, the carbon nanofibers, or a combination of the two; the five additional models are shown in Figure 7. The effective thermal conductivity models are expressed in the following:

$$k_{e,[R//(CF-CNF)]} = k_R V_R + \frac{(V_{CF} + V_{CNF})^2}{(V_{CF}/k_{CF}) + (V_{CNF}/k_{CNF})}, \quad (9)$$

$$k_{e,[CNF//(CF-R)]} = k_{CNF} V_{CNF} + \frac{(V_{CF} + V_R)^2}{(V_{CF}/k_{CF}) + (V_R/k_R)}, \quad (10)$$

$$k_{e,[CF-(R//CNF)]} = \frac{1}{(V_{CF}/k_{CF}) + \left((V_R + V_{CNF})^2/(k_R V_R + k_{CNF} V_{CNF})\right)}, \quad (11)$$

$$k_{e,[R-(CF//CNF)]} = \frac{1}{(V_R/k_R) + \left((V_{CF} + V_{CNF})^2/(k_{CF} V_{CF} + k_{CNF} V_{CNF})\right)}, \quad (12)$$

$$k_{e,[CNF-(R//CF)]} = \frac{1}{(V_{CNF}/k_{CNF}) + \left((V_R + V_{CF})^2/(k_R V_R + k_{CF} V_{CF})\right)}. \quad (13)$$

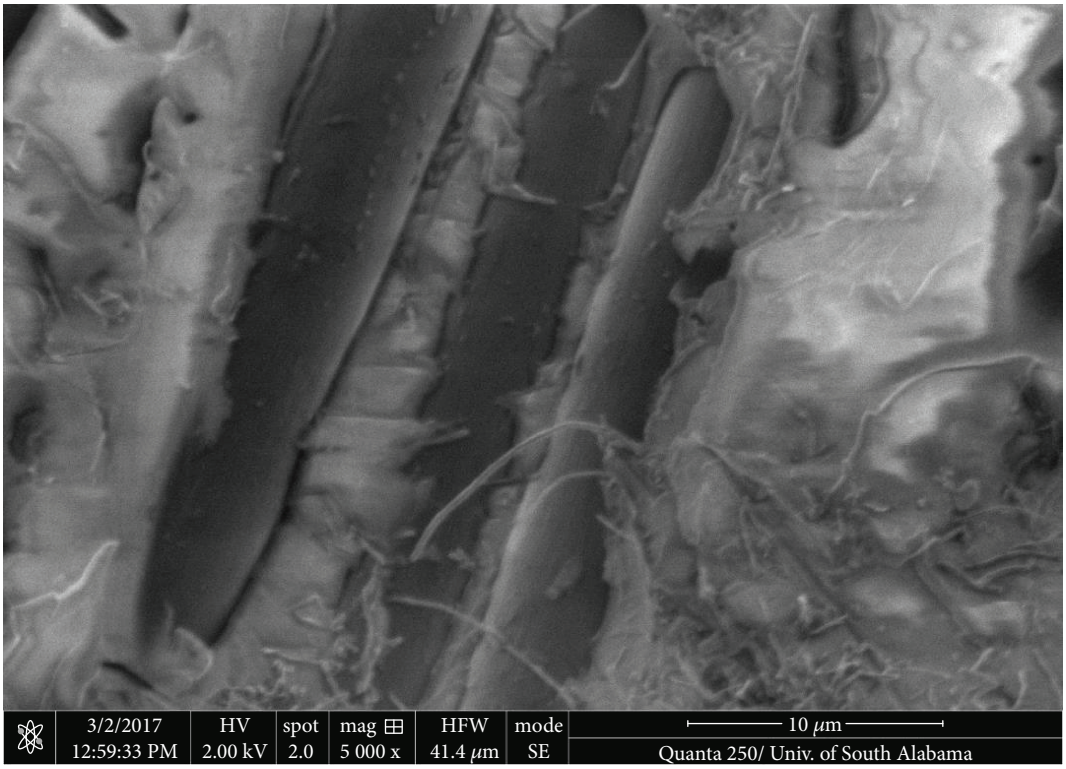

Figure 4: 1 wt% UA-CFRP delamination surface (top view).

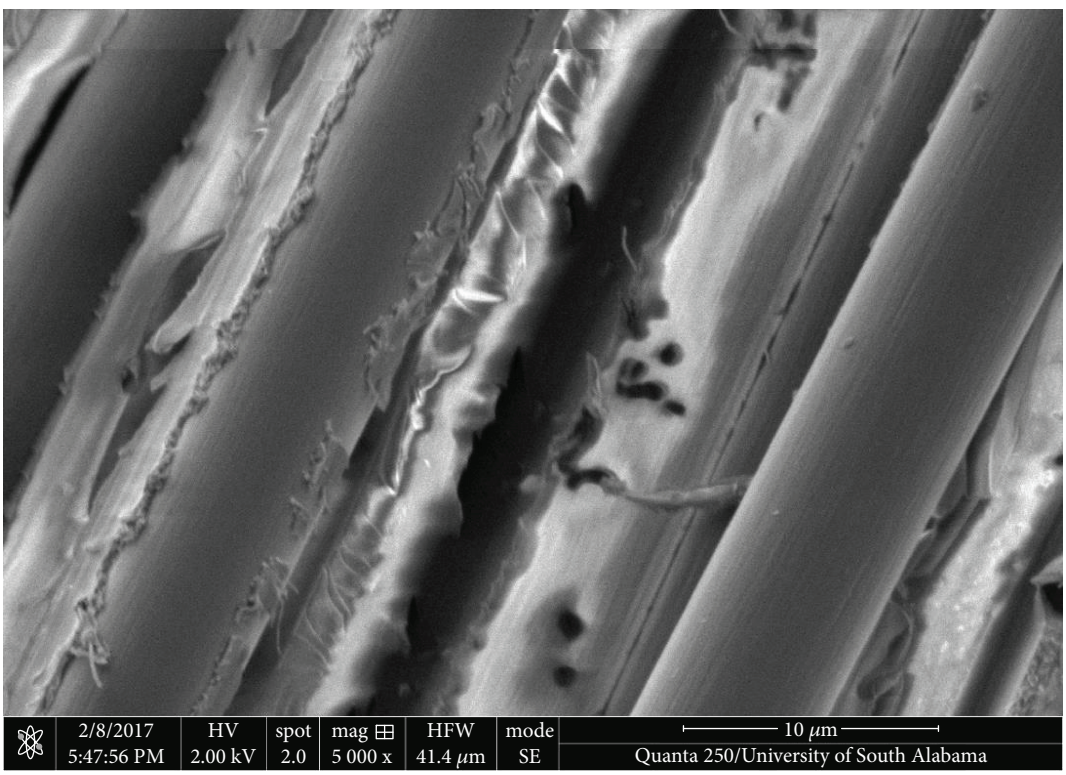

Figure 5: 1 wt% ZT-CFRP delamination surface (top view).

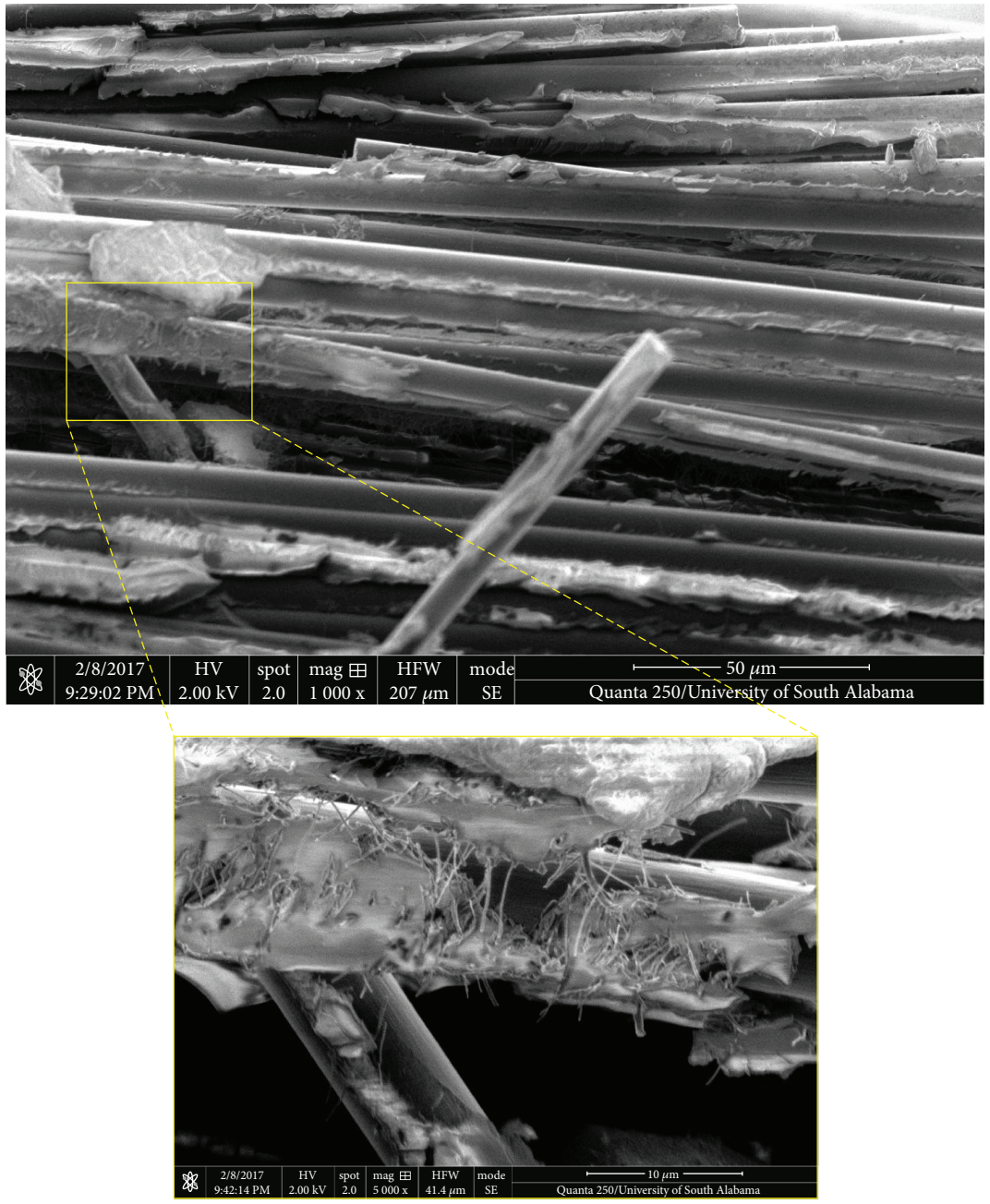

Figure 6: 1 wt% ZT-CFRP delamination surface (oblique view).

Table 3 compares the experimental thermal conductivity results with the predicted results from all the proposed models.

As expected, the Series model [CF-R] made the most accurate prediction for the control CFRP; note that, in the absence of CNF, Model [CNF//(CF-R)], Model [CF-(R//CNF)], and Model [R-(CF//CNF)] are equivalent to the Series model [CF-R]. For the UA-CFRP, both Model [control CFRP//CNF] and Model [CNF//(CF-R)] made accurate predictions. A comparison of these two resistor-models illustrates that both models have the CNFs as a parallel resistor to the CFRP composite; the two models only differ in the way they treat the CFRP components, which can either be decomposed into a CF-R structure or left as an intact CFRP. In both scenarios, the highly conductive CNF directly adds a parallel conductive pathway that enhances the overall conductivity of the composite. However, the CNF in these cases cannot penetrate the layer of insulating resin that envelops the carbon fibers, and thus, the high conductivity of the carbon fibers cannot be effectively utilized in the UA-CFRP.

For the ZT-CFRP, the Parallel model [CF//R//CNF], Model [R//(CF-CNF)], Model [CF-(R//CNF)], and Model [CNF-(R//CF)] made predictions that were very close to the experimental data. A comparison of these four resistor-

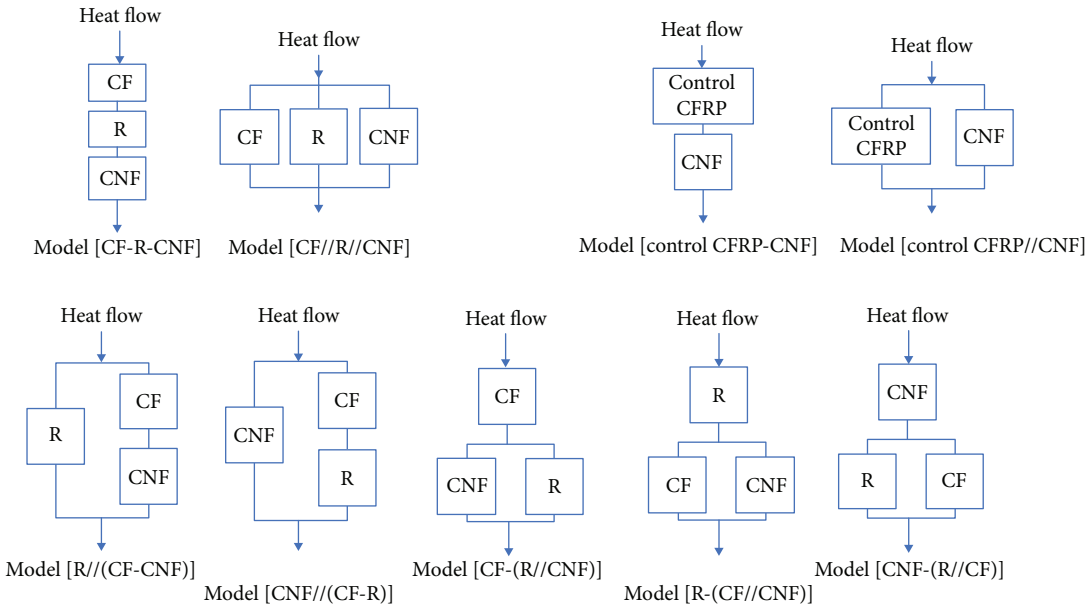

Figure 7: Various resistor-based thermal conductivity models used to test the possible synergy among carbon fibers, resin, and carbon nanofibers in the UA-CFRPs and ZT-CFRPs.

Table 3: Comparison of the experimental thermal conductivity results and the predicted results from various models, wherein the modeling results with relative errors less than 50% are shown in bold.

Experimental data		$k_{e,\text{ControlCFRP}}$ (W/m-K)		$k_{e,\text{UA-CFRP}}$ (W/m-K)	$k_{e,\text{ZT-CFRP}}$ (W/m-K)
		1.31		3.61	9.85
Modeling Data	$k_{e,\text{Control CFRP}}$ (0 wt% CNF) (W/m-K)	$\frac{k_{e,\text{Model}}}{k_{e,\text{Exp}}}$	$k_{e,\text{CFRP with CNF}}$ (1 wt% CNF) (W/m-K)	$\frac{k_{e,\text{Model}}}{k_{e,\text{Exp}}}$	$\frac{k_{e,\text{Model}}}{k_{e,\text{Exp}}}$
Series model [CF-R-CNF]	0.76	**58%**	0.77	21%	8%
Parallel model [CF//R//CNF]	8.26	631%	11.39	316%	**116%**
Model [control CFRP//CNF]	—	—	4.44	**123%**	45%
Model [control CFRP-CNF]	—	—	1.31	36%	13%
Model [R//(CF-CNF)]	8.26	631%	8.30	230%	**84%**
Model [CNF//(CF-R)]	0.76	**58%**	3.89	**108%**	40%
Model [CF-(R//CNF)]	0.76	**58%**	11.39	316%	**116%**
Model [R-(CF//CNF)]	0.76	**58%**	0.78	22%	8%
Model [CNF-(R//CF)]	8.26	631%	8.29	230%	**84%**

models illustrates that all four models allow the carbon fiber (i.e., CF resistor) to effectively connect to both ends of the thermal circuit, which is accomplished either by itself (Parallel model [CF//R//CNF]) or by a link with the highly conductive CNF (Model [R//(CF-CNF)], Model [CF-(R//CNF)], and Model [CNF-(R//CF)]). Each of these four models allows the heat flow to largely bypass the highly resistive resin. However, as previously stated, all individual carbon fibers are enveloped by the resin, which indicates that Parallel model [CF//R//CNF], Model [R//(CF-CNF)], and Model [CNF-(R//CF)] are not possible. Therefore, the only possibility that remains to represent the ZT-CFRP is Model [CF-(R//CNF)]. Note that the prediction made by Model [CF-(R//CNF)] was only 0.00204% less than the Wiener upper bound (predicted by Parallel model [CF//R//CNF]); this indicates that the ZT-CFRP has a very effective thermal transport structure.

According to this study, the models that best represent the control CFRP, UA-CFRP, and ZT-CFRP are Series model [CF-R], Model [CNF//(CF-R)], and Model [CF-(R//CNF)], respectively. By analyzing these three models, one can find that the role of the resin is always linked in series with carbon fiber, whereas the role of the CNF is always linked in parallel with the system. Moreover, in the ZT-CFRP, the CNF penetrates through the insulating resin and releases the potential of the carbon fiber, which illustrates the synergetic role of CNF z-threads in through-thickness

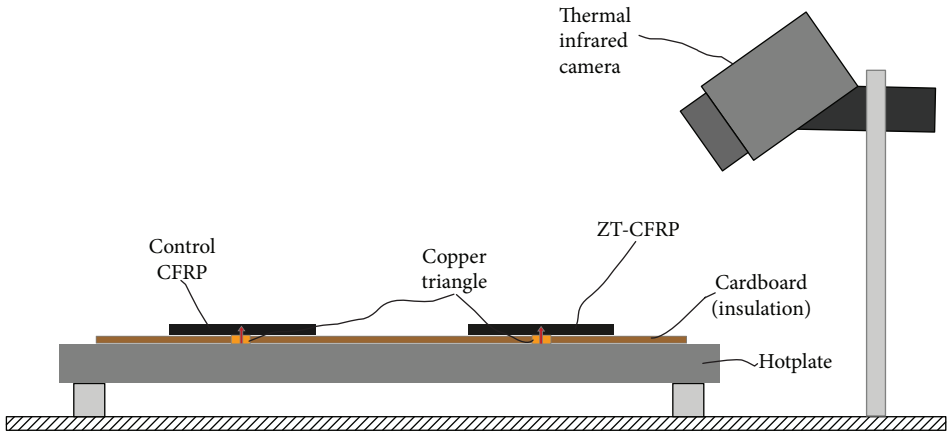

Figure 8: Schematic of the thermal infrared test setup.

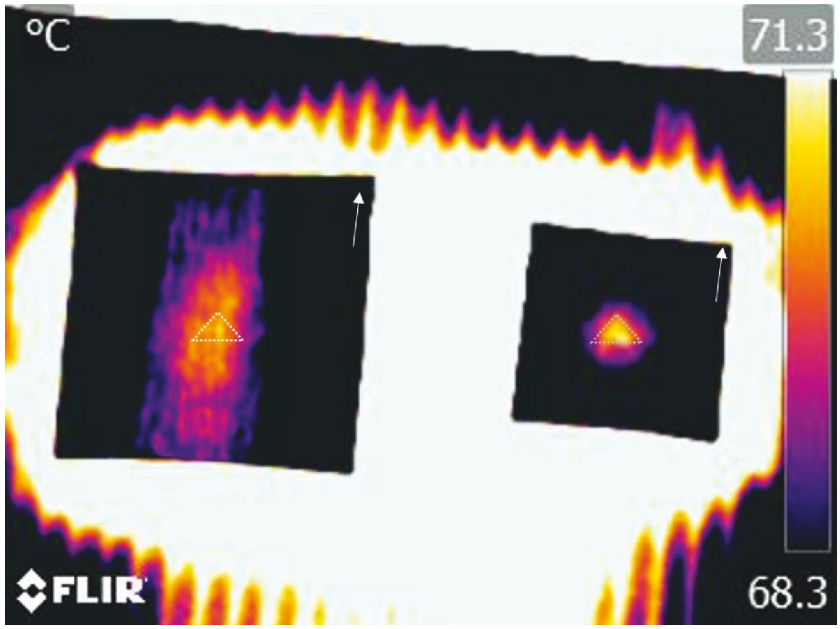

Figure 9: Thermal image of control CFRP (left) and ZT-CFRP (right). Note that the white arrows represent the longitudinal direction of the carbon fibers within each CFRP.

thermal transport; note that the thermal conductivity of the ZT-CFRP approaches the Wiener upper bound of Parallel model [CF//R//CNF].

3.4. Enhanced Defect Detection in ZT-CFRPs. Thermal infrared inspection is a nondestructive testing method used to evaluate defects (e.g., voids, delaminations) within CFRPs. Taking thermal infrared images of composites is a fast noncontact method that can provide information about the interior structure of the composite [29]. Defects within a structure affect the local thermal conductivity, which subsequently changes the thermal images of the composite; these changes make it possible to detect defects within the composite. However, the anisotropic nature of CFRPs makes it challenging to locate the defects and accurately ascertain their respective shapes. As such, it was hypothesized that CFRPs with more isotropic thermal conductivity would help locate and visualize defects within CFRPs, which could lead to greater repair accuracies and thus reduce repair costs.

To test the aforementioned hypothesis, a simple test setup was prepared that involved a thermal infrared camera (FLIR E40 60 Hz), a hotplate heated to 100°C, cardboard (used as insulation), and a small copper triangle (dimensions: 10 mm × 10 mm × 14 mm). Note that the copper triangle was used to represent a centralized defect within the composite since defects transmit different heat flux compared with the rest of the composite. A schematic of the test setup is shown in Figure 8.

Figure 9 shows the thermal image of the control CFRP (left) and the ZT-CFRP (right). The position of the triangle is marked with a dashed line. Note that the ZT-CFRP has smaller dimensions since it was cut to an appropriate size to measure its electrical conductivity [17], which was used to validate the z-threading manufacturing process.

As shown in Figure 9, it is much easier to accurately locate and visualize the defect (i.e., the copper triangle) within the ZT-CFRP than it is within the control CFRP. These results validate the hypothesis that the nearly isotropic thermal conductivity of the ZT-CFRP helps locate defects and determine their respective geometries during thermal infrared testing. Future studies could perform additional tests to gain more knowledge about the improved infrared testing capabilities of ZT-CFRPs.

4. Conclusions

In this study, the through-thickness conductivity of CFRPs reinforced with CNF z-threads was determined using a steady-state parallel plate testing device. At 1 wt% CNF concentration in the matrix (approximately 0.2 vol% of the CFRP), ZT-CFRPs had a through-thickness thermal conductivity of 9.85 W/m-K, which is approximately 7.53 times as conductive as control CFRPs constructed from the same fiber/matrix system and approximately 2.73 times as conductive as CFRPs with unaligned CNF reinforcement of the same concentration. Accordingly, the CNF z-threads were found to play a substantial role in increasing the through-thickness thermal conductivity of CFRPs.

To better understand the role of the CNF z-threads in through-thickness thermal transport, simple logical models of the CFRPs were constructed and then compared with the experimental results. Through these analyses, it was determined that the CNF z-threads substantially enhance the through-thickness thermal conductivity of a CFRP by creating carbon fiber-CNF linkages throughout the laminate as described by Model [CNF-(R//CF)]; these linkages allow the heat flow to largely bypass the resistive resin that envelops the carbon fibers. Moreover, in the ZT-CFRP, the CNF penetrates through the insulating resin and releases the potential of the carbon fiber, which illustrates the synergetic role of CNF z-threads in through-thickness thermal transport; note that the thermal conductivity of the ZT-CFRP approaches the Wiener upper bound (illustrated by Parallel model [CF//R//CNF]).

At 9.85 W/m-K, the thermal conductivity of the 1 wt% ZT-CFRPs approaches the lower limits of commercially available stainless steel. Furthermore, it draws near to the in-plane thermal properties of CFRPs of approximately 10 W/m-K [4]. This relatively high thermal conductivity allows ZT-CFRPs to more readily replace traditional metals in applications that encounter high thermal loads. In addition, the nearly isotropic thermal properties of the ZT-CFRPs help locate internal defects during thermal infrared testing, which can improve repair accuracy and thus lower repair costs. Moreover, the high thermal conductivity of ZT-CFRPs will help to reduce thermal gradients during cure processes, which can increase uniformity and reduce residual thermal stresses caused by thermal gradients and nonuniform curing. As such, CNF z-threads enable the curing of thicker CFRP parts, as well as faster curing cycles. These findings highlight the emergent impact of CNF z-threads on the composite industry.

Data Availability

The composite thermal conductivity measurements, the SEM images, the modeling equations, and thermal infrared images data used to support the findings of this study are included within the article. Previously reported CFRP and CNF z-threaded CFRP composite prepreg manufacturing process data were used to support this study and are available at [doi:10.1016/j.compositesa.2016.10.022]. These prior studies (and datasets) are cited at relevant places within the text as references [16].

Disclosure

The work presented within this article is an extension of the thesis published by Alexander M. Scruggs at the University of South Alabama [18].

Conflicts of Interest

The manufacturing method for the CNF z-threaded CFRP prepreg is disclosed in the patent application titled "Method for manufacturing nanostructurally aligned multiscale composites" (WO2015017321 A1 (first published in Feb 5, 2015), CN 105517781 B, CN105517781A, EP3027390A1, EP3027390A4, US20160168342); this manufacturing method was invented by Kuang-Ting Hsiao and Gregory Hickman.

Acknowledgments

The authors are grateful for the financial support provided by Hexcel Corporation and for the discussions and suggestions from Paul Mackenzie, David Tilbrook, Alex Baidak, and Kenneth Smith. In addition, the authors would like to acknowledge the support provided by the Alabama-EPSCoR GRSP Program (Grant no. 150436), the National Science Foundation (Grant nos. 1158862 and 1748369), and the Alabama Department of Commerce (Grant no. 150436).

References

[1] P. K. Mallick, *Fiber-Reinforced Composites: Materials, Manufacturing, and Design*, CRC Press, 3rd edition, 2007.

[2] M. Ashby, *Materials Selection in Mechanical Design*, Butterworth-Heinemann, 5th edition, 2017.

[3] R. Rolfes and U. Hammerschmidt, "Transverse thermal conductivity of CFRP laminates: a numerical and experimental validation of approximation formulae," *Composites Science and Technology*, vol. 54, no. 1, pp. 45–54, 1995.

[4] N. Yamamoto, R. Guzman de Villoria, and B. L. Wardle, "Electrical and thermal property enhancement of fiber-reinforced polymer laminate composites through controlled implementation of multi-walled carbon nanotubes," *Composites Science and Technology*, vol. 72, no. 16, pp. 2009–2015, 2012.

[5] "Pyrograf I," Applied Sciences Inc., http://apsci.com/?page_id=17.

[6] "HexTow AS4 Carbon Fiber," Hexcel, http://www.hexcel.com/user_area/content_media/raw/AS4_HexTow_DataSheet.pdf.

[7] "Cryogenic material properties 304 Stainless," NIST, https://trc.nist.gov/cryogenics/materials/304Stainless/304Stainless_rev.htm.

[8] K.-Y. Park, S.-E. Lee, C.-G. Kim, and J.-H. Han, "Application of MWNT-added glass fabric/epoxy composites to electromagnetic wave shielding enclosures," *Composite Structures*, vol. 81, no. 3, pp. 401–406, 2007.

[9] L. Jin, C. Bower, and O. Zhou, "Alignment of carbon nanotubes in a polymer matrix by mechanical stretching," *Applied Physics Letters*, vol. 73, no. 9, pp. 1197–1199, 1998.

[10] F. H. Gojny, M. H. G. Wichmann, U. Kopke, B. Fiedler, and K. Schulte, "Carbon nanotube-reinforced epoxy-composites: enhanced stiffness and fracture toughness at low nanotube content," *Composites Science and Technology*, vol. 64, no. 15, pp. 2363–2371, 2004.

[11] C. Kostagiannakopoulou, E. Fiamegkou, G. Sotiriadis, and V. Kostopoulos, "Thermal conductivity of carbon nanoreinforced epoxy composites," *Journal of Nanomaterials*, vol. 2016, Article ID 1847325, 12 pages, 2016.

[12] E. J. Garcia, B. Wardle, A. Johnhart, and N. Yamamoto, "Fabrication and multifunctional properties of a hybrid laminate with aligned carbon nanotubes grown *in situ*," *Composites Science and Technology*, vol. 68, no. 9, pp. 2034–2041, 2008.

[13] S. S. Wicks, R. G. de Villoria, and B. L. Wardle, "Interlaminar and intralaminar reinforcement of composite laminates with aligned carbon nanotubes," *Composites Science and Technology*, vol. 70, no. 1, pp. 20–28, 2010.

[14] S. S. Wicks, W. Wang, M. R. Williams, and B. L. Wardle, "Multi-scale interlaminar fracture mechanisms in woven composite laminates reinforced with aligned carbon nanotubes," *Composites Science and Technology*, vol. 100, pp. 128–135, 2014.

[15] R. Li, N. Lachman, P. Florin, H. D. Wagner, and B. L. Wardle, "Hierarchical carbon nanotube carbon fiber unidirectional composites with preserved tensile and interfacial properties," *Composites Science and Technology*, vol. 117, pp. 139–145, 2015.

[16] K.-T. Hsiao, A. M. Scruggs, J. S. Brewer Jr, G. J. S. Hickman, E. E. McDonald, and K. Henderson, "Effect of carbon nanofiber z-threads on mode-I delamination toughness of carbon fiber reinforced plastic laminates," *Composites Part A: Applied Science and Manufacturing*, vol. 91, no. 1, pp. 324–335, 2016.

[17] A. M. Scruggs, K. Henderson, and K.-T. Hsiao, "Characterization of electrical conductivity of a carbon fiber reinforced plastic laminate reinforced with z-aligned carbon nanofibers," in *Proceedings of CAMX 2016*, p. TP16-0137, Anaheim, CA, September 2016.

[18] A. M. Scruggs, *Enhancement of Through-Thickness Electrical Conductivity due to Carbon Nanofiber Z-Threads in Unidirectional Carbon Fiber Reinforced Plastic Laminates [M.S. Thesis]*, Department of Mechanical Engineering, University of South Alabama, Mobile, Alabama, 2018.

[19] "Pyrograf-III carbon nanofiber," *e-Business Express*2011, http://pyrografproducts.com/nanofiber.html#_PR-24-XT-PS_Data_Sheet.

[20] K.-T. Hsiao and S. Gangireddy, "Investigation on the spring-in phenomenon of carbon nanofiber-glass fiber/polyester composites manufactured with vacuum assisted resin transfer molding," *Composites Part A: Applied Science and Manufacturing*, vol. 39, no. 5, pp. 834–842, 2008.

[21] A. M. Scruggs, S. Kirmse, and K.-T. Hsiao, "Influence of z-aligned carbon nanofibers on the through-thickness thermal conductivity of paraffin wax," in *Proceedings of ASME IMECE 2016*, p. V008T10A081, Phoenix, AZ, USA, November 2016, Paper No. IMECE2016-67795, http://proceedings.asmedigitalcollection.asme.org/proceeding.aspx?articleid=2602604.

[22] H. Yin, X. Gao, J. Ding, and Z. Zhang, "Experimental research on heat transfer mechanism of heat sink with composite phase change materials," *Energy Conversion and Management*, vol. 49, no. 6, pp. 1740–1746, 2008.

[23] E. Kandare, A. A. Khatibi, S. Yoo et al., "Improving the through-thickness thermal and electrical conductivity of carbon fibre/epoxy laminates by exploiting synergy between graphene and silver nano-inclusions," *Composites Part A: Applied Science and Manufacturing*, vol. 69, pp. 72–82, 2015.

[24] S. Han, J. T. Lin, Y. Yamada, and D. D. L. Chung, "Enhancing the thermal conductivity and compressive modulus of carbon fiber polymer–matrix composites in the through-thickness direction by nanostructuring the interlaminar interface with carbon black," *Carbon*, vol. 46, no. 7, pp. 1060–1071, 2008.

[25] S. Han and D. D. L. Chung, "Increasing the through-thickness thermal conductivity of carbon fiber polymer–matrix composite by curing pressure increase and filler incorporation," *Composites Science and Technology*, vol. 71, no. 16, pp. 1944–1952, 2011.

[26] J. L. Abot, G. Bardin, C. Spriegel, Yi Song, V. Raghavan, and N. Govindaraju, "Thermal conductivity of carbon nanotube array laminated composite materials," *Journal of Composite Materials*, vol. 45, no. 3, pp. 321–340, 2009.

[27] "Product bulletin EPIKOTE™ resin 862/EPIKURE™ curing agent W system," Miller-Stephenson, https://www.miller-stephenson.com/wp-content/uploads/2016/08/W.pdf.

[28] P. B. Kaul, M. F. P. Bifano, and V. Prakash, "Multifunctional carbon nanotube-epoxy composites for thermal energy management," *Journal of Composite Materials*, vol. 47, no. 1, pp. 77–95, 2013.

[29] R. UnnÞòrsson, M. T. Jonsson, and T. P. Runarsson, "NDT methods for evaluating carbon fiber composites," in *Proceedings of the Composites Testing and Model Identification*, pp. 21–23, Bristol, UK, 2004.